

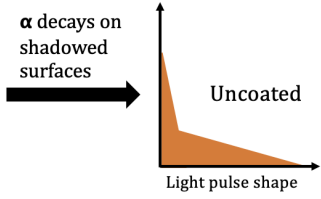
Graphical Abstract

Development and characterization of a slow wavelength shifting coating for background rejection in liquid argon detectors

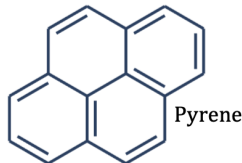
D. Gallacher, A. Leonhardt, H. Benmansour, E. Ellingwood, Q. Hars, M. Kuźniak, J. Anstey, B. Bondzior, M. G. Boulay, B. Cai, P. J. Delfano, S. Garg, J. Mason, T. R. Pollmann, P. Skensved, V. Strickland, M. Stringer

Problem

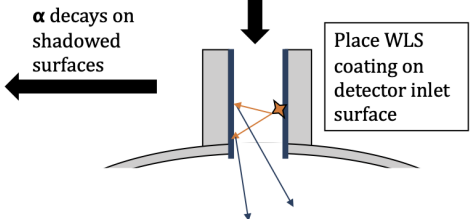
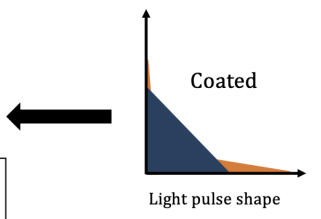
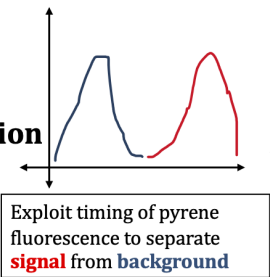
Backgrounds in a liquid argon detector



Characterization of a wavelength shifter for use inside a LAr detector to target backgrounds



Solution



Highlights

Development and characterization of a slow wavelength shifting coating for background rejection in liquid argon detectors

D. Gallacher, A. Leonhardt, H. Benmansour, E. Ellingwood, Q. Hars, M. Kuźniak, J. Anstey, B. Bondzior, M. G. Boulay, B. Cai, P. J. Delfano, S. Garg, J. Mason, T. R. Pollmann, P. Skensved, V. Strickland, M. Stringer

- Wavelength shifter characterization
- Background rejection techniques for liquid argon detectors
- Cryogenic detector technologies

Development and characterization of a slow wavelength shifting coating for background rejection in liquid argon detectors

D. Gallacher^{a,*}, A. Leonhardt^d, H. Benmansour^b, E. Ellingwood^b, Q. Hars^b, M. Kuźniak^{c,a,f}, J. Anstey^a, B. Bondzior^e, M. G. Boulay^a, B. Cai^{a,3}, P. J. Dereń^e, P. C. F. Di Stefano^b, S. Garg^a, J. Mason^a, T. R. Pollmann^{d,2}, P. Skensved^{b,f}, V. Strickland^a and M. Stringer^{b,f}

^aDepartment of Physics, Carleton University, Ottawa, K1S 5B6, ON, Canada

^bDepartment of Physics, Engineering Physics & Astronomy, Queen's University, Kingston, ON, K7L 3N6, Canada

^cAstroCeNT, Nicolaus Copernicus Astronomical Center, Polish Academy of Sciences, Rektorska 4, 00-614 Warsaw, Poland

^dDepartment of Physics, Technische Universität München, 80333 Munich, Germany

^eInstitute of Low Temperature and Structure Research, Polish Academy of Sciences, Okólna 2, 50-422 Wrocław, Poland

^fArthur B. McDonald Canadian Astroparticle Physics Research Institute, Queen's University, Kingston ON K7L 3N6, Canada

ARTICLE INFO

Keywords:

Wavelength shifters
Liquid Argon
Dark Matter
TPB
Pyrene
Background Rejection

ABSTRACT


We describe a technique, applicable to liquid-argon-based dark matter detectors, allowing for discrimination of alpha-decays in detector regions with incomplete light collection from nuclear-recoil-like events.

Nuclear recoils and alpha events preferentially excite the liquid argon (LAr) singlet state, which has a decay time of ~ 6 ns. The wavelength-shifter TPB, which is typically applied to the inside of the active detector volume to make the LAr scintillation photons visible, has a short re-emission time that preserves the LAr scintillation timing. We developed a wavelength-shifting polymeric film - pyrene-doped polystyrene - for the DEAP-3600 detector and describe the production method and characterization. At liquid argon temperature, the film's re-emission timing is dominated by a modified exponential decay with time constant of 279(14) ns, and has a wavelength-shifting efficiency of 46.4(2.9) % relative to TPB, measured at room temperature. By coating the detector neck (a region outside the active volume where the scintillation light collection efficiency is low) with this film, the visible energy and the scintillation pulse shape of alpha events in the neck region are modified, and we predict that through pulse shape discrimination, the coating will afford a suppression factor of $\mathcal{O}(10^5)$ against these events.

1. Introduction

Liquid argon (LAr) is used as a scintillator for the detection of particles in many applications. These include fundamental physics experiments for direct dark matter detection (DEAP [1], DarkSide [2], MiniCLEAN [3]) and neutrino detection (DUNE [4], MicroBooNE [5], LArIAT [6]). LAr scintillation light has a wavelength peaked in the vacuum ultraviolet (VUV) at ~ 128 nm, below the peak efficiencies of available photo-sensors. Wavelength shifters (WLS) are materials that efficiently absorb VUV light and then re-emit it at a longer wavelength. This emission is typically isotropic and in the blue-visible region, where commercially available photo-sensors are most sensitive. It has been shown [7–10] that in addition to wavelength shifting, WLS coatings with scintillation decay-times sufficiently different from the LAr excimer decay-time can be used to effectively reject surface- α backgrounds in LAr detectors. In this work, we demonstrate how the wavelength shifting process itself can be used to reject alpha backgrounds originating from regions in the detector that have incomplete light collection. We describe here the development and characterization of a polymeric, WLS-doped thin-film for the rejection of alpha backgrounds from areas with limited light collection efficiency that is suitable for deployment in a liquid argon environment.

*Corresponding author

 dgallacher@sno1lab.ca (D. Gallacher)

ORCID(s): 0000-0002-9395-0560 (D. Gallacher)

¹Currently at McGill University, Montréal, Quebec H3A 2T8, Canada

²Currently at Nikhef and the University of Amsterdam, Science Park, 1098XG Amsterdam, Netherlands

³Currently at the Office of Research Services, Queen's University, Kingston, Ontario K7L 3N6, Canada

1.1. Wavelength shifters

The most common WLS for LAr applications is the organic wavelength shifter 1,1,4,4-tetraphenyl-1,3-butadiene (TPB), chosen because of its high conversion efficiency ($\sim 100\%$ [11]), fast re-emission time $\mathcal{O}(ns)$ [12], and long-term stability [13, 14]. TPB is an example of an organic WLS; other examples include pyrene [15], p-Terphenyl [16], and polyethylene naphthalate [17], for a recent review see [18].

When an incident UV photon interacts with the WLS molecule, the WLS molecule is excited from the singlet ground state, S_0 , into a vibrational level of a higher-energy state. The excited state can then decay down to a lower-lying state through internal conversion ($\mathcal{O}(ns)$), vibrational relaxation ($\mathcal{O}(ps)$), or undergo a transition to a triplet state ($\mathcal{O}(ns)$). The latter is suppressed due to its classically spin-forbidden nature. Transitions from $S_1 \rightarrow S_0$ occur on $\mathcal{O}(ns)$ timescales and emit fluorescence, transitions from $T_1 \rightarrow S_0$ occur on longer timescales ($\mathcal{O}(\mu s - ms)$), due to the spin-forbidden nature, and produce phosphorescence. Energy loss due to internal conversion and vibrational transitions results in a wavelength shift from high energy UV light to lower energy fluorescence and phosphorescence light. At room temperature, the molecule may be in a vibrationally excited state, which leads to overlap between the absorption and emission spectra.

WLS are broadly characterized by the following properties:

- Emission spectrum and peak wavelength(s), $\lambda_{E,max}$
- Photo-luminescent quantum yield (PLQY), characterized by the ratio of emitted photons/absorbed photons
- Re-emission lifetime(s), τ

For operation in LAr detectors, the vapour pressure is also an important WLS characteristic; a low vapour pressure is necessary to prevent material loss, and the WLS must exhibit cryogenic and long-term stability for continued operation at 87 K.

Most of the above characteristics will exhibit some dependence on temperature. At lower temperatures, vibrational modes are "frozen-in" resulting in a smaller overlap between absorption and emission spectra, and PLQY tends to increase as thermal quenching of excited states is reduced.

While TPB is the WLS material of choice for conversion of the primary scintillation light in LAr detectors, other WLS materials show strong potential for specific use within LAr applications. Pyrene is one such WLS material, and has been studied extensively in the past for different applications [19]. The crystal structure of pyrene is dimeric in form, and the elementary unit of the lattice is a pair of pyrene molecules. The fluorescence spectrum of pyrene has attributes of monomer ($\lambda_{E,max}^m \sim 375$ nm) and excimer ($\lambda_{E,max}^e \sim 450$ nm) emission, while the absorption spectrum is characteristic of monomer absorption [19]. Monomers that are initially excited by UV light will rapidly convert into excimers which decay through fluorescence with a lifetime of $\mathcal{O}(100$ ns), and because the nature of this interaction is dependent on the presence of neighbouring pyrene monomers, there is a strong dependence on the number density of pyrene.

TPB films can be applied to materials such as acrylic by thermal deposition [20]. Due to its higher vapour pressure of 6×10^{-6} mbar [21], a pyrene film created by thermal deposition is not stable for LAr applications where a high vacuum is required before filling. However, pyrene-doped polymers, such as polystyrene (PS), have been studied extensively [22, 23]. Mobility of pyrene molecules in the polymeric matrix is very strongly constrained, which is reflected by the diffusion constant of pyrene in PS, $D=9.4 \cdot 10^{-19}$ cm²/s, one of the lowest ever measured [24]. Therefore, films with good PLQY and vacuum stability are feasible.

1.2. Background rejection with a slow WLS

Pulse shape discrimination (PSD) is used in LAr detectors to separate electron-recoil (ER) backgrounds, such as the beta decay of ³⁹Ar, from the nuclear-recoil (NR) WIMP signal events. Alpha decays in LAr have a scintillation time structure that is too similar to that of the expected dark matter signal for PSD to discriminate them. While alpha decays inside the fiducial volume can be discriminated against WIMP recoils based on their much higher energy, those that occur in a region of the detector with incomplete light collection, such as in detector inlets, can reconstruct at low energies, so that they appear in the WIMP search region both in energy and in PSD space. This is a limiting background in the DEAP-3600 experiment [25].

The DEAP-3600 acrylic vessel (AV) has a neck at the top through which evaporated argon gas flows up toward a cooling coil to be liquefied again. This inlet contains so called "flowguides" - a set of acrylic components meant to direct the LAr and gaseous argon (GAR) flow. The flowguides are showered with LAr droplets from the cooling

coil, which is believed to create a thin LAr film. Radon progeny on the surface of the flowguides undergo α -decay, causing VUV scintillation light in this LAr film. Most of the scintillation light is absorbed by the bare acrylic of the flowguides, but a small fraction of the light makes its way into the AV, where it is wavelength shifted by a layer of TPB and then detected by the inner photo-detectors. Since most of the event's scintillation light is shadowed by the flowguides, the reconstructed energy of these events is much smaller than the true energy, so that some of these events appear in the low-energy WIMP search region. Simulations of this configuration reproduce the unique features observed in the detector data [25, Section VII-D3].

The shadowed α scintillation events and expected pulse shape are illustrated in Figure 1 (top). Due to the fast re-emission time of the TPB coating on the inside of the AV, the pulse shape is determined by the LAr singlet (approximately 6 ns) and triplet (approximately 1300 ns to 1600 ns) excimer states. By coating the flowguide surfaces with a thin WLS film, VUV light from α scintillation in LAr from this region will be wavelength shifted, so that it can be detected by the PMTs. This increases the reconstructed event energy, moving the events out of the WIMP energy region of interest. Furthermore, choosing a WLS with a slow time response shifts some prompt LAr scintillation photons to later times. This moves the events away from the WIMP search region of interest in PSD space. With its $\mathcal{O}(100\text{ ns})$ time constant, pyrene is a suitable candidate to achieve the desired distortion in the pulse shape. We will discuss the PSD power against shadowed α 's achievable by a pyrene coat in Sect. 4, after describing the production and characterization of pyrene films.

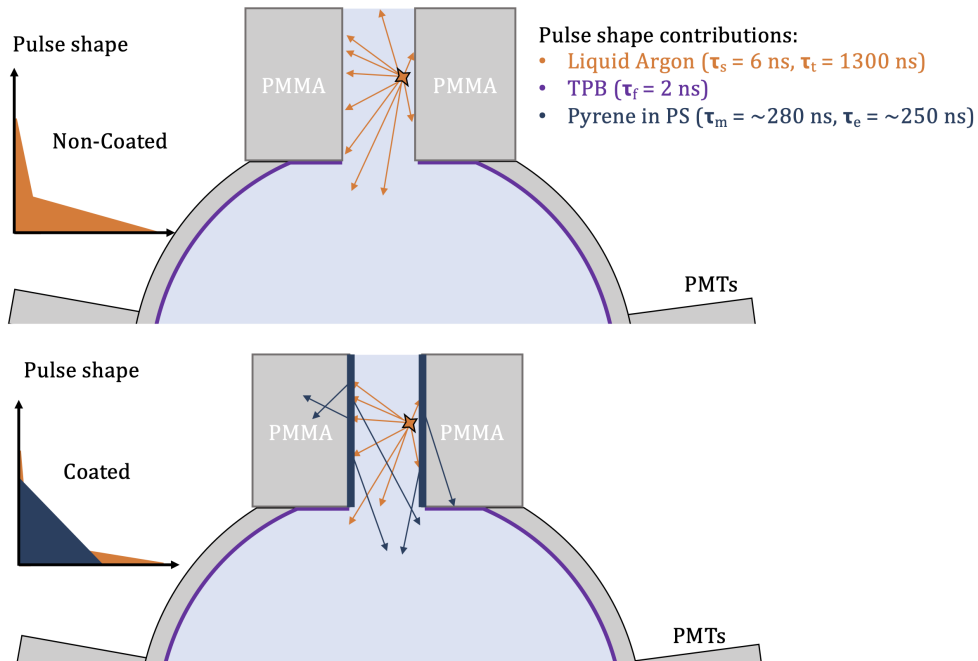


Figure 1: Top: α scintillation event occurs in the neck of the DEAP-3600 detector, VUV scintillation light is absorbed by the acrylic of the neck and produces a shadowed low energy, highly prompt event that mimics a potential dark matter signal. Bottom: VUV light from α scintillation in argon is absorbed by the pyrene + PS film coating and is shifted to visible and delayed by the time constant of the film. This produces events with a strong "intermediate" component that can be tagged efficiently using PSD, as illustrated by the inlaid pulse shapes.

2. Film Preparation

We prepared films with 5% through 25% of pyrene dissolved in polymethyl methacrylate (PMMA), polyvinyltoluene (PVT), and polystyrene, applied to acrylic by painting with a brush, by pour and set, and by dipping. Based on the characterization of the films, which is described in section 3, a film composed of PS, doped with 15% pyrene (PPS film hereafter), was selected as the optimal WLS for the DEAP-3600 neck. The film preparation technique detailed

Development and characterization of a slow wavelength shifting coating for background rejection in liquid argon detectors here, and the characterization results presented in Section 4 therefore focus on this combination.

2.1. Production of pyrene-doped polystyrene films

The procedure for preparing the PPS film is detailed below. All steps except the cleaning are carried out in a nitrogen-purged glove-box to prevent oxidation of the pyrene film. It is critical for the stability of the film to keep the pyrene and the PPS film isolated from oxygen and moisture and to reduce exposure to UV light, as this was observed to have a deteriorating effect on the quality of the coating. All WLS films were prepared onto a sanded and cleaned acrylic substrate.

1. Sonicate polystyrene beads in ultra-pure water (UPW) and Alconox solution then rinse with UPW to remove any surface contamination
2. Using a clean beaker, add 15% pyrene⁴ by weight
3. Add 85% polystyrene beads⁵ by weight
4. Add toluene to beaker (changing the volume of toluene relative to the solids will effect the viscosity of the film for application, for our application we use 1.0 g of solids to 3.0 mL of toluene for a paint-able viscosity)
5. Placing beaker on a hot-plate with a magnetic stir stick, heat to 75 °C and stir at medium velocity for 15 minutes (solids will dissolve if left in toluene without heat or stirring after several hours)
6. Remove beaker from hot plate and let cool for 15 minutes
7. Using a nylon bristled brush, apply coating to sample surface
8. Wait 48 hours for coating to set before handling
9. If a thicker coating is desired, several coats can be applied by repeating steps 2-7 after initial coating has set for several hours

While not in use, samples were stored in dark and sealed containers.

The following samples were produced for characterization:

1. Single-coat and double-coat, 98% purity PPS samples used for cryogenic tests at Carleton University, with thicknesses of 10-50 μm
2. Single-coat, 99% purity (9 μm), 98% purity (8 μm), and double-coat 98% purity (19 μm) PPS samples sent to the Technical University of Munich (TUM)
3. Single-coat, 15% pyrene of 99.9% purity in: PVT (73 μm), PMMA (65 μm) sent to TUM
4. Single-coat, 15% pyrene concentration, PPS samples with purities of: 99.9% (50 μm), 99% (12 μm), and 98% (15 μm), sent to Queen's University
5. Single-coat, 12% pyrene concentration, 99.9% purity (55 μm) PPS sample sent to Queen's University
6. Single-coat, 98% purity (16 μm) PPS sample sent to Institute of Low Temperature and Structure Research of the Polish Academy of Sciences (ILTSR)

2.2. TPB reference sample production

TPB reference samples were prepared in a thermal vacuum deposition chamber at Carleton University, described in [7]. The TPB was loaded into a porcelain crucible wrapped with a nichrome heating element with a Pt100 temperature sensor attached. Temperature data was sent to a Lakeshore monitor that controls the current supply of the heating element to maintain a constant temperature set at the desired deposition rate. The deposition is monitored with a quartz crystal monitor located next to the sample, 18 cm above the crucible, and read out with a custom Labview program. The TPB was first cycled to evaporation at 240 °C (measured at the heating element) to prevent sputtering. The acrylic substrates were prepared in the same manner as those used for the PPS samples. After sanding and cleaning, the samples were loaded into the vacuum chamber. The chamber was evacuated to $<10^{-4}$ mbar. Deposition proceeded at a rate of 1-2 $\text{\AA}/\text{s}$ at 240 °C for 2.5 hours, resulting in a thickness of $\sim 1 \mu\text{m}$. All TPB samples used by TUM, Queen's and ILTSR were prepared in the same deposition and stored in a dark container within a nitrogen-purged glove box for one week until shipment to the respective institutions.

⁴Sigma-Aldrich 82648-10G (CAS# 129-00-0, fluorescence grade)

⁵Scientific Polymer Cat# 400 (CAS# 9003-53-6)

3. Characterization of films

The PPS film will be used at LAr temperature (approximately 84 K) and will have to shift LAr scintillation light into the visible regime. Thus, we need to determine the cryogenic stability of the coating itself, as well as the photoluminescence timing, spectrum, and quantum yield (PLQY). The PLQY will be measured relative to the PLQY of the TPB reference samples.

3.1. Mechanical and cryogenic stability

Samples with varying concentrations of pyrene were produced, those with concentrations greater than 18% pyrene by mass displayed severe crystallization of pyrene during curing and were not pursued further.

Two different cryogenic tests were carried out; in the first, samples of pyrene with PS, PMMA, PVT were placed inside a LAr cryostat at Carleton University [26] and held for 2 months. Of the 3 classes of samples, only PS samples showed no visible cracking or coating degradation. In the second test, 1" acrylic disks coated with different thicknesses of PS were slowly cooled by lowering samples into LN₂ vapour space until eventually submerging. No macroscopically visible cracking was observed for any of the PPS samples, regardless of thickness or number of coats. Close inspection of samples under a compound microscope showed micro-cracking of the film at the $\mathcal{O}(1-10\ \mu\text{m})$ scale. These micro-cracks were stable under moderate mechanical stress, and no material loss was observed for any samples during subsequent cryogenic cycling of samples.

3.2. Photoluminescence properties

Measurements of photoluminescence response at cryogenic temperature and in the VUV wavelength regime are notoriously difficult and prone to systematic uncertainties. Therefore, we use three separate setups: the optical cryostat at Queen's University, described in [27] and in [28] (excitation with 285 nm photons, sample at cryogenic temperatures), the VUV setup at TUM described in [29] (excitation with 128 nm photons, sample at room temperature), and the VUV setup at ILTSR (excitation with 128 nm photons, sample at cryogenic temperature).

3.2.1. Decay time constant

The fluorescence decay time constants of 15% PPS film samples were studied at 300 K and at 87 K using the optical cryostat at Queen's University. The setup consists of a closed-cycle optical cryostat capable of reaching temperatures between 4 K and 300 K with a pressure $<10^{-6}$ mbar. A 285 nm UV LED is set up outside the optical cryostat window to provide a $\lesssim 10$ ns FWHM excitation pulse that interacts with the sample within the cryostat chamber. For this study, the UV LED light interacts with the pyrene coating on an acrylic substrate. Outside the cryostat exit window there is a 375–650 nm broadband filter to prevent any stray UV LED light from reaching the photodetector. Additional filters were used in measurements to study the separate contributions from the pyrene monomer (effectively a 400 nm shortpass) and excimer (455 nm longpass) fluorescence components to the overall pyrene fluorescence. The fluorescent light from the sample is then detected by a Hamamatsu R6095 PMT with a super-bialkali photocathode. The setup is described in detail in [28].

At each temperature, the data set consists of 45 000 waveforms of the fluorescence pulse from the pyrene sample measured by the PMT. The data analysis of these time-resolved measurements are done using the average pulse of all the waveform pulses in the data set. Full experimental details, along with analysis over a broader range of temperatures, will be presented elsewhere, with details available in Ref. [28].

3.2.2. Emission Spectrum

To characterize the WLS emission spectrum and intensity, we use the TUM VUV setup, with the following modifications from [29]: the deuterium lamp was replaced with model H2D2 L15094 from Hamamatsu, and for the characterization of the final film, the sample chamber was replaced for better control of the sample angle and optimized light collection. All measurements were done at room temperature and wavelength-resolved with an OceanInsight QE65000 spectrometer. The response of the light detection system, composed of the lens, optical fiber, and spectrometer, was calibrated with a reference light source. The setup is described in detail in [30].

The following measurement protocol was followed: The monochromator entrance and exit slits were opened to 5 mm and a wavelength of 130 nm was selected on the monochromator. At the chosen slit width, the wavelength resolution is approximately 12 nm. After installing the sample in the sample holder, the sample chamber was closed and the setup was evacuated to a pressure of 5×10^{-4} mbar or better. The deuterium lamp was then turned on and reached stable light intensity after 1 min. Sample spectra were measured 10 times for 20 s each and then averaged.

Each measurement of a WLS sample spectrum was preceded by a measurement of the TPB reference. Spectra were corrected for dark-noise and for the wavelength-dependent response function of the photon detection system, and then integrated between 350 nm to 650 nm to obtain the emission intensity. We consider three sources of uncertainty: a) the uncertainty on the dark noise level, b) system instability, and c) the uncertainty on the response function of the light detection system. Assuming that the TPB reference sample did not degrade over the time-frame of these measurements, we take as the system instability the RMS over the individual measurements of the TPB emission intensity. With the original sample holder, the system instability over one week of measurements was approximately 3%. With the new sample holder, this decreased to 1%. The uncertainty on the response function of the photon detection system is given by the RMS over several calibrations, and is treated as a systematic uncertainty common to all measurements.

The emission spectrum was also measured with the setup at ILTSR lab, with limited resolution due to cryogenic equipment reducing light collection efficiency.

3.2.3. Photoluminescence Yield

The relative PLQY of PPS at 80 K with respect to room temperature was measured for excitation with 128 nm photons at ILTSR. The setup consists of a McPherson vacuum monochromator and spectrophotometer supplied with a deuterium lamp (EXW Herrsching L1835), a PMT (Hamamatsu R928) and a longpass filter (Schott WG320).

The system is also equipped with an optional cold-finger cryostat (KrioSystem 03020) permitting to cool down the sample.

Furthermore, the relative PLQY of PPS with respect to TPB was extracted from the pulse shapes recorded with the Queen's optical cryostat, albeit at a higher wavelength. The amplitude of each of the 45 k waveforms was integrated over a three-microsecond window containing the main peak and the decay. The integrated amplitude distribution for all events was then fitted by a skew normal distribution whose mean was associated with the average amount of light.

The relative PLQY was finally also extracted from the spectra measured with the TUM VUV setup. Each sample's PLQY with respect to a TPB reference was calculated by taking the ratio of the integrated spectra in a window from 350 nm to 650 nm.

4. Results

4.1. Photoluminescence Time Constants

The photoluminescence pulse shapes of the monomer and excimer emissions of the 15% PPS (50 μm) film are fitted with a function that is the convolution of the UV excitation pulse timing with the photoluminescence decay model $i(t)$ to extract the decay time constants.

The monomer pulse shape can be represented using a decay model described in detail in [22]:

$$i_m(t) = \frac{N_1}{\tau_1} \exp\left(-\frac{t}{\tau_1} - 2q\sqrt{\frac{t}{\tau_1}}\right), \quad (1)$$

where τ_1 is the monomer lifetime, and the $\sqrt{t/\tau}$ term is proportional to the excimer formation time. An example of the monomer decay fit at 87 K is shown in Figure 2. The figure also shows the relative residuals $\frac{\text{data-model}}{\text{model}}$.

The pulse shape of the excimer-only photoluminescence is not well-described by a single exponential decay term. We use the following fit model:

$$i_e(t) = -\frac{N_{\text{rise}}}{\tau_{\text{rise}}} e^{-\frac{t}{\tau_{\text{rise}}}} + \frac{N_2}{\tau_2} e^{-\frac{t}{\tau_2}} + \frac{N_3}{\tau_3} e^{-\frac{t}{\tau_3}} \quad (2)$$

This model includes two decay terms representing two different populations of excimers, τ_2 and τ_3 (where $\tau_3 > \tau_2$) and one rise time τ_{rise} corresponding to the excimer formation time.

An example of the excimer decay fit at 87 K is shown in Figure 3.

Decay times obtained from those fits are summarized in Table 1.

Errors of $\pm 5\%$ were attributed to the decay time values to account for the systematic and statistical errors from the fit.

The combined efficiencies of the optical filters of the PMT in the monomer and excimer wavelength ranges are ϵ_m and ϵ_e , respectively. At each temperature, we calculate the total photoluminescence intensity as $I_t = N_1/\epsilon_m + (N_2 + N_3)/\epsilon_e$. The fractional contribution of the monomer and the two excimer states to the PLQY is then calculated as

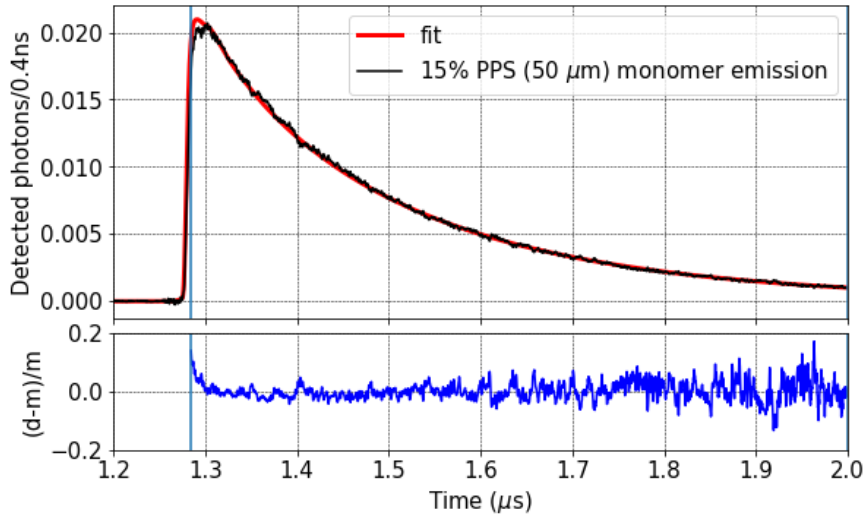


Figure 2: Fit of the pyrene monomer photoluminescence decay at 87 K using model from Equation 1 in a [1285 ns - 2000 ns] fitting window

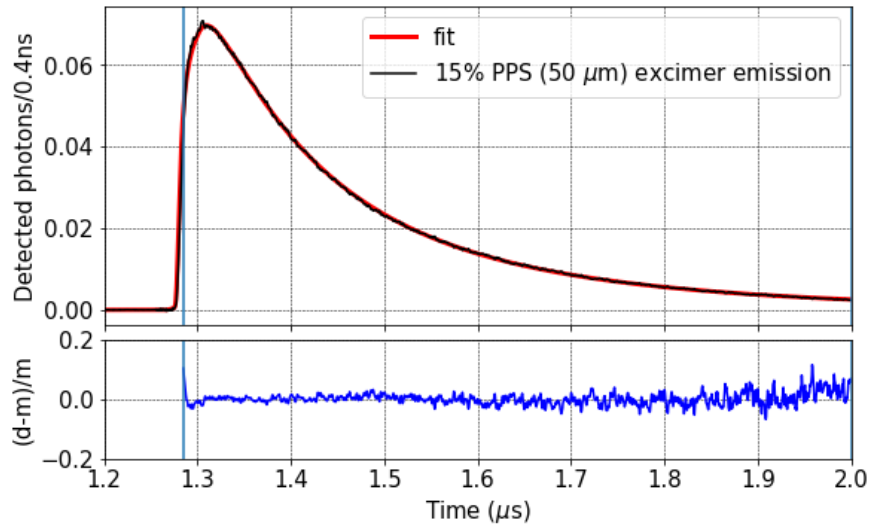


Figure 3: Fit of the pyrene excimer photoluminescence decay at 87 K using the model from Equation 2 in a [1285 ns - 2000 ns] fitting window

$F_1 = \frac{N_1/\epsilon_m}{I_t}$, $F_2 = \frac{N_2/\epsilon_e}{I_t}$, $F_3 = \frac{N_3/\epsilon_e}{I_t}$ and summarized in Table 2. The contribution of the rise-time (N_{rise}) is treated as a systematic uncertainty.

4.2. Photoluminescence Yield and Emission Spectrum

The room temperature spectra of three WLS samples and of the TPB reference excited with 128 nm photons using the TUM setup are shown in Figure 4. The spectral shapes and intensities of the three PPS samples studied at TUM matched within uncertainties. We show results from the sample with 9 μm thickness here.

Each sample's relative PLQY with respect to a TPB reference was calculated by taking the ratio of the integrated spectra in a window from 350 nm to 650 nm. The relative yields for a set of samples using different polymeric matrix materials are shown in Table 3.

We use the pulse shapes measured in the Queen's optical cryostat to study the evolution of the PLQY with tem-

Table 1
Photoluminescence decay times of 15% PPS (50 μm)

	Monomer	Excimer (Short)	Excimer (Long)
Temp. (K)	τ_1 (ns)	τ_2 (ns)	τ_3 (ns)
300	214(11)	91(5)	194(10)
87	279(14)	105(5)	249(12)

Table 2
Fractions of PLQY (F_i) contributed by the monomer and the two excimer decays for 15% PPS (50 μm).

	Monomer	Excimer (Short)	Excimer (Long)
Temp. (K)	F_1 (%)	F_2 (%)	F_3 (%)
300	23(6)	36(9)	43(10)
87	52(13)	18(5)	31(8)

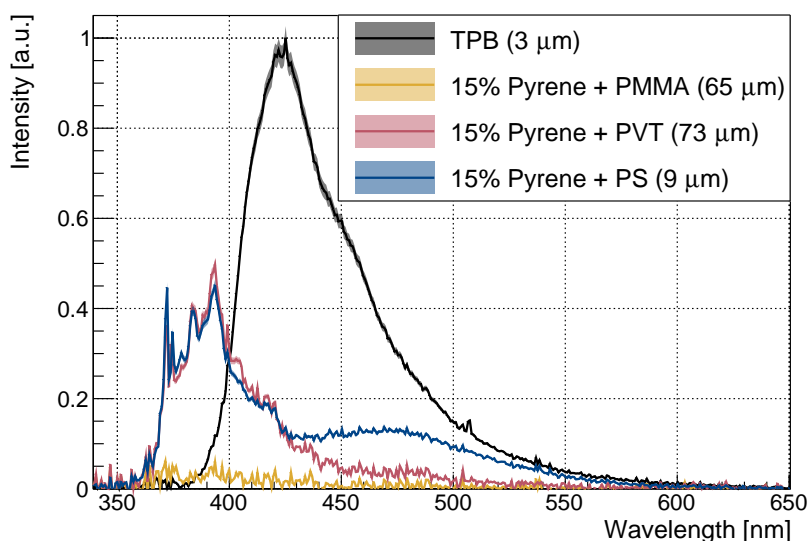


Figure 4: The spectra recorded at room temperature for three samples of 15% pyrene in different polymeric matrices with 128 nm excitation are shown together with the TPB reference spectrum. The shaded regions indicate the size of the statistical uncertainties related to the dark noise correction and the system fluctuation.

peratures. The pulse shape from each of the 45 000 recorded events was integrated in a three-microsecond window containing the main peak and the decay. The integrated intensity distribution for all events was then fitted by a skew normal distribution whose mean was associated with the average amount of light.

For PPS (50 μm), the PLQY increases by 7(1)% when cooling from room temperature to 87 K, while the TPB film's PLQY increases by 19(2)%.

Given a PPS/TPB PLQY ratio of 59(6)% at RT, this translates into a PPS/TPB PLQY ratio of 53(6)% at 87 K. This result is shown in the second-to-last column of Table 3.

Using the ILTSR setup, the monomer excitation spectrum shown in Figure 5 exhibits strong increase below 150 nm as well as less pronounced bands at 175, 245 and 270 nm. Consistent with other measurements, the emission spectrum recorded at 128 nm consists of dominant monomer and excimer peaks at 396 and 475 nm, respectively.

The PPS spectra measured at RT and at 80 K using the ILTSR setup are shown in Figure 5 and Figure 6. The low resolution of the low temperature spectra is due to the sample cooling system, which degrades the light collection efficiency. The temperature dependence of the response of the setup was calibrated using samples of TPB and polyethylene naphthalate (PEN) WLS's, which have known [31, 32] ratios of low-temperature and room-temperature

Table 3

This table summarizes the measurements of the relative photoluminescence yield of 15% pyrene in PMMA, PVT, and PS (the latter is referred to as 'PPS' in the text) samples with respect to the TPB reference sample. Values in grey are taken from samples as measured at TUM, due to limited resolution at ILTSR, with scaling applied as measured.

Sample	PLQY w.r.t. TPB [%]			
	80 K to 87 K		room temp.	
	128 nm	285 nm	128 nm	285 nm
Pyrene + PMMA (65 μm)			3.7(0.5)	
Pyrene + PVT (73 μm)			34.9(2.7)	
PPS (9 μm)			46.4(2.9)	
PPS (50 μm)		53(6)		59(6)
PPS (16 μm)	36(6)		46.4	

Table 4

This table summarizes the intensity ratio of the excimer and monomer emission at 128 nm and 285 nm, for room and LAr temperatures. Values in grey are taken from samples as measured at TUM, due to limited resolution at ILTSR.

Sample	Excimer/Monomer Intensity			
	80 K to 87 K		room temp.	
	128 nm	285 nm	128 nm	285 nm
PPS (9 μm)			0.43 (0.05)	
PPS (50 μm)		0.9 (0.3)		3.4 (1.1)
PPS (16 μm)	0.47		0.43	

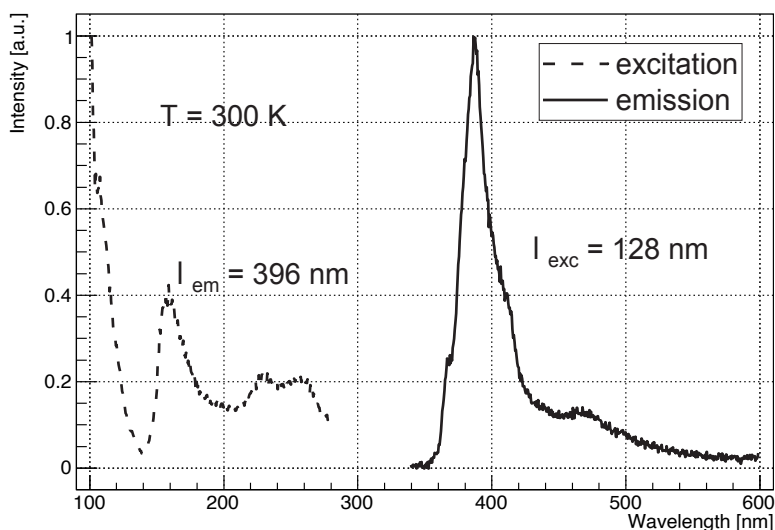


Figure 5: Excitation and emission spectra for a 15% PPS coating, measured at room temperature. The excitation spectrum (left) shows the monomer emission intensity at 396 nm as a function of the excitation wavelength. The emission spectrum (right) was measured at 128 nm.

PLQY at 128 nm excitation. Consistent calibration factors were obtained from both materials.

The relative PLQY change between room temperature and 80 K at 128 nm excitation wavelength was obtained by integrating the spectra in the 370–420 nm range for the monomer, 450–500 nm for the excimer emission, and 370–500 nm for the overall factor.

The PLQY of the monomer at 80 K decreased by $-25(10)\%$, while that of the excimer decreased by $-17(14)\%$, making the intensity of the total emission spectrum decrease by $-23(11)\%$ compared to the RT value.

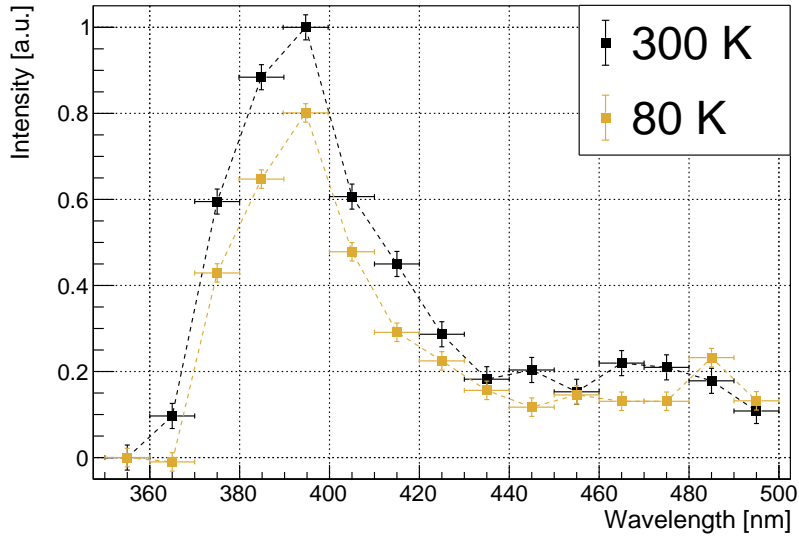


Figure 6: Emission spectra of a 15% PPS (16 μm) sample at 128 nm excitation wavelength, at 300 K and 80 K, measured at ILTSR. Collected with the sample installed in the cryostat.

Table 5
Input parameters for simulation

Input Component	Model	Parameters	Reference
LAr pulse shape	2-exponential + Intermediate	$\tau_s = 2.2 \text{ ns}$, $\tau_l = 1445 \text{ ns}$, $\tau_I = 75.5 \text{ ns}$	[33]
PPS pulse shape	3-exponential	Table 1 & Table 2	This article
TPB pulse shape	Volt-Laustriat + 2-exponential	See Table 1 in Ref.	[33]
α Energy	Mono-energetic	5.3 MeV	[34]
NR Energy	Uniform Distribution	50-250 keV	Assumed
Shadowing Fraction	Uniform Distribution	50-100%	Assumed
PMT Efficiency	Measurement	Mean of 30%	[35]
TPB Emission Spectrum	Measurement	Mode at $\sim 420 \text{ nm}$	This article (Figure 4)
PPS Emission Spectrum	Measurement	Mode at $\sim 390 \text{ nm}$	This article (Figure 4)
PPS PLQY	Measurement	0.46/0.36	This article (Table 3)

4.3. Predicting the background discrimination efficiency

A toy Monte-Carlo simulation was carried out to estimate the expected background discrimination efficiency with a PPS coated inlet, as illustrated in Figure 1. Input parameters for the simulation are summarized in Table 5.

4.3.1. Simulation details

The simulation assumes that the full energy of the 5.3 MeV α particle is stopped in the LAr at the inlet, which was confirmed for a 50 μm LAr film with SRIM [36]. The energy is converted into an expected number of photons based on the liquid argon light yield of $\sim 40\text{k ph/MeV}$ with an α quenching factor of 0.71 [37]. The number of photons produced for each α event is sampled from a Gaussian with a mean equal to the number of expected photons \times quenched energy deposition and a sigma equal to the square root of the mean. Since true α events from the inlet will have an admixture of both LAr and wavelength shifted light from the PPS coating, the number of photons produced is split into two parts by sampling a "shadow fraction" from a uniform distribution from 50% to 100%. The "shadowed fraction" represents the solid angle effect of the inlet, where the shadowing fraction represents the shadowing from the inlet geometry, and "non-shadowed" photons that represent the light from the inlet that enters the detector bulk directly without interacting with the WLS coating. All photons are given a delay time sampled from a liquid argon pulse

shape described by [33] with parameters tuned for NR-like signals. Assuming that TPB is a 100% efficient wavelength shifter [12], non-shadowed photons are then given a TPB wavelength and delay time sampled from distributions as described in Table 5. Shadowed photons have a probability of being shifted by the PPS film, using the value of PLQY from this article, shown in Table 2, photons that are successfully shifted are then given a delay time sampled from the pulse shape given in Eq. 1, and Eq. 2 with parameters given in Table 1 and a wavelength sampled from the PPS distribution shown in Figure 4 for PPS (9 μm). Shadowed photons are then given a 50% probability of being transmitted into the detector and subsequently detected, corresponding to the solid angle effect of being in the inlet. A 400 nm cut-off is imposed on all photons to simulate the absorption from the acrylic light-guides and acrylic vessel, and geometric broadening is imposed by adding a delay time to each photon sampled from a Gaussian with parameters from [33]. After imposing these conditions, the wavelength of each photon is used to determine the detection probability using the wavelength dependent efficiency of the Hamamatsu R5912-HQE PMTs used by DEAP-3600 [35], if the photon is successfully detected its hit-time is added to a data-structure for subsequent analysis. Each detected photon has a probability to produce an after-pulse with parameters given by [33], if an after-pulse is registered an additional hit is triggered with a delay time sampled from the after-pulsing distribution in [33], modelled by a sum of Gaussian distributions.

For comparison to WIMP-like NR LAr scintillation signals for background rejection efficiency determination, the same simulation was carried out for a 50-250 keV uniform energy deposition of NR-like signals, with no shadowing or PPS photons produced.

4.3.2. Simulation Results

Comparison of the simulated pulse shapes for inlet α 's with a PPS coating as described in this note to an expected pure LAr pulse shape for WIMP-like NR signals are shown in Figure 7.

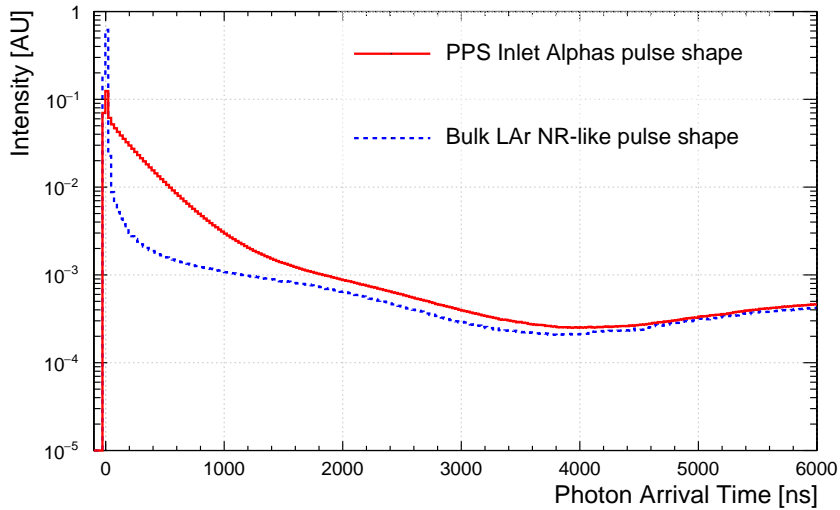


Figure 7: Comparison of pulse shapes for NR-like LAr events and inlet α 's with a PPS coating from TMC, where both distributions are normalized to unit integral. The distributions include contributions from the LAr pulse shape, TPB re-emission and PMT effects. The rise in intensity starting at 4000 ns is due to PMT afterpulsing.

A common PSD parameter is defined as the fraction of total light detected in a “prompt” window Equation 3,

$$F_{\text{prompt}} = \frac{\sum_{t_{\text{start}}}^{t_{\text{prompt}}} N(t)}{\sum_{t_{\text{start}}}^{t_{\text{end}}} N(t)} \quad (3)$$

where for discrimination against ^{39}Ar beta decays: $t_{\text{start}} = -28$ ns, $t_{\text{prompt}} = 60$ ns, and $t_{\text{end}} = 10\,000$ ns (for full details, refer to [38]). For discrimination against shadowed α 's with a PPS coating on the flowguides, we use $t_{\text{prompt}} = 40$ ns and call this discriminator ‘Fpyrene’.

The Fpyrene parameter windows were tuned by scanning over integration windows for both NR-like and PPS inlet- α simulations, while to first-order window boundaries can be found graphically by looking for the crossing points of the normalized PDF's of the pulse shapes in Figure 7.

The distributions of Fpyrene for simulated NR-like signals and PPS inlet- α 's are shown in Figure 8. To avoid assumptions about the accuracy of the energy scale of the toy simulation, we only consider the PPS inlet- α 's that fall in the lowest quartile of the PPS inlet- α energy distribution (measured in number of hit photons), which is nearest to the region of interest for WIMP searches. As there is an inverse relationship between the reconstructed energy of an event and the amount of shadowing present for that event, which with a PPS-coated inlet leads to an increase in "pyrene-like" slow photons in the PMT hit distribution, the lowest energy events reconstruct lower in Fpyrene.

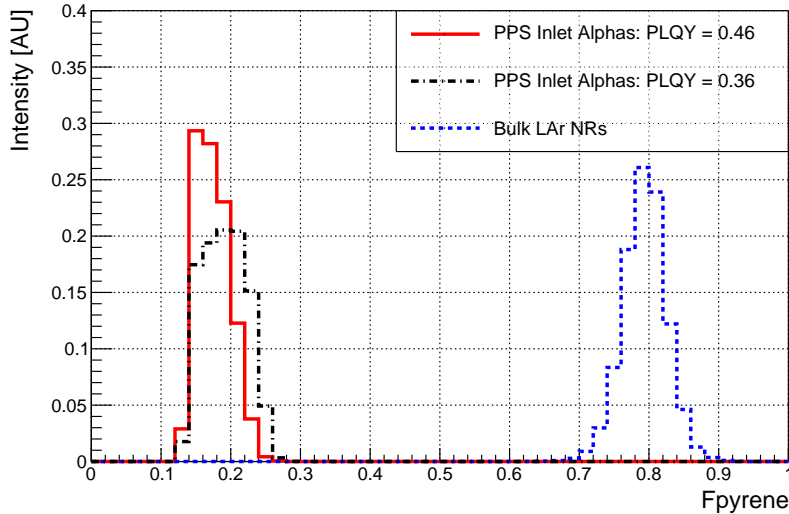


Figure 8: Fpyrene distributions for pure LAr NR-like signals and low-energy shadowed PPS coated inlet α 's. Both nominal PLQY and lower bound for inlet α 's are shown, with lower bound from ILTSR, all distributions are normalized to unit integral

The PSD leakage fraction is defined as the fraction of PPS inlet α 's that will leak into the region of NR-like LAr events, and is described in Equation 4. We consider the full energy distribution of NR-like LAr events, and assume 100% acceptance.

$$LF_{90\%C.L.} = \frac{\left(\sum_{i=e}^{N_{bins}} F_{pyrene}^{PPS} [i] \right)_{90\% C.L.}}{N_{Evs}} \quad (4)$$

The upper limit on leakage into the ^{40}Ar NR region of interest for nominal PLQY is [$< 1.2 \times 10^{-5}$] $_{90\% C.L.}$, assuming 100% NR signal acceptance. The conservative lower bound on the PPS PLQY with reduction measured at ILTSR was applied and is shown in Figure 8, no events are observed to leak into the region of interest.

5. Discussion

We produced wavelength-shifting coatings that consist of pyrene embedded in a polymer matrix (PMMA, PVT, or PS) on a sanded acrylic substrate. The coatings were tested for their wavelength-shifting response and for mechanical stability in a cryogenic environment, and a coating composed of 15% pyrene and 85% polystyrene (PPS) by weight was identified as a candidate for use in the DEAP-3600 detector upgrade.

After undergoing cryogenic cycling, the candidate coating did show some microscopic crazing at the $\mathcal{O}(1 \mu\text{m})$ scale. The crazing did not lead to de-lamination or material loss even when subjected to further cryogenic cycling, and the optical transmission at visible wavelengths was unaffected. The mechanical stability of the PPS films after cryogenic

cycling indicates that the bond between the PPS film and the sanded acrylic substrate is stronger than the PPS itself. This is likely caused by the use of toluene as the solvent for the PPS film, which will also dissolve the acrylic surface and would lead to a material interface between the PPS film and acrylic that is a homogenous mixture of the PPS and acrylic. This acts as a strong bond for the material. Therefore, we expect this coating to be stable under operation in a LAr environment.

Three different setups were used to characterize the photoluminescence response of the PPS film, because of their complementary capabilities and as cross-check for each other's results. For technical reasons, PPS films of different thicknesses were characterized in the three setups. We checked that the coating thickness has negligible influence on the results. The wavelength ranges that could be used for the PPS monomer and excimer emission are also slightly different between setups. This introduces a discrepancy up to 6% in the reported relative PLQY values.

We find that the PPS film has a pulse shape characterized by the exponential decays of a monomer and of two excimer states. The relative abundances and lifetimes of the three states are presented in Table 1 and Table 2. At 87 K and for excitation with 285 nm photons, the monomer, which has a lifetime of 279 ns, dominates the emission intensity, followed by the excimer state with 249 ns lifetime. Thus, the majority of photons are re-emitted with a suitable timing approximately 50 times larger than the LAr singlet excimer decay time. The decay times of the pyrene excited states are independent of the excitation wavelength, as long as this wavelength is below the emission spectrum of the pyrene. However, the fractional contribution of the excimer and monomer states to the total pulse-shape as outlined in Table 2 can be different at the LAr scintillation wavelength of 128 nm if there is a pyrene density gradient in the film, because the 285 nm photons penetrate deeper into the film than the 128 nm photons. We observe that the excimer over monomer intensity ratio decreases strongly when going from 285 nm to 128 nm excitation light, both for the measurements at room temperature and at cryogenic temperature (since only the Queen's setup can separate the two excimer components, only their sum is considered for comparisons with the other results). This indicates that the density of pyrene molecules is lower near the film surface, so that when the pyrene there is excited, it has less chance of finding another molecule to form an excimer with before it decays.

We measured the PLQY of the PPS film relative to the PLQY of a TPB film that is similar to the film on the DEAP-3600 detector vessel. The PLQY of TPB has previously been reported to increase by 22(13)% when going from RT to 87 K [31] under excitation with 128 nm photons. This is consistent with the 19(2)% increase measured using the Queen's optical cryostat. The photon detection efficiency of the ILTSR device has a temperature dependence that had to be calibrated by determining a scaling factor that requires the TPB emission intensity ratio between RT and 80 K to match the literature value. The calibration was confirmed by measuring the PLQY of a second WLS with known behaviour at cryogenic temperatures. The discrepancy between the behaviour of the PPS film's PLQY at cryogenic temperatures between the Queen's and the ILTSR measurement can have several explanations: 1) The behaviour of the PPS film at cryogenic temperatures could differ between the two excitation wavelengths. 2) Sample-to-sample differences lead to a wavelength or temperature-dependent effect, for example, different scattering behaviour at the surfaces of the samples. 3) The monomer's contribution to the total emission intensity increases at low temperatures, especially under excitation with 285 nm light. The monomer's wavelength range covers a region where both the PMT used at Queen's and the spectrometer used at ILTSR have steep efficiency curves. A small inaccuracy in the calibration of the response of the light detection system can thus lead to large differences in results.

We consider the difference between the two measured values for the relative PLQY at cryogenic temperature as the size of the systematic uncertainty on this value.

The PPS and TPB emission spectra measured here and shown in Figure 4 are used as input to a toy Monte Carlo simulation. The RT spectra for 128 nm excitation photons are used because the change of the spectral shape for this excitation wavelength is not significant when going to cryogenic temperatures, and the resolution is better than for the spectra shown in Figure 6. The simulation also accounts for the measured PPS pulse shape and the PPS PLQY relative to TPB, as well as for the wavelength-dependent photon detection efficiency and instrumental noise of the DEAP-3600 light detection system.

The simulations indicate that by using pulse shape discrimination together with the PPS film on the detector inlet, the inlet- α background rate can be reduced by a factor of better than 1.2×10^{-5} , while not rejecting any potential WIMP events.

The effect of the newly introduced inlet coatings on events in the inner detector can be estimated by considering the relative surface area of the pyrene coated surface to the TPB coated inner vessel. The neck of the DEAP acrylic vessel subtends a solid angle of $\sim 1\%$ from the centre of the vessel and since to first order only half of the WLS light from the PPS coating will transit back down into the detector, the expected contribution of "pyrene-like" photons to

an inner detector event is minimal. If we assume activities as reported in Ref. [25], without evaluating second order effects and cut efficiencies, this technique is sufficient to operate the DEAP-3600 detector for ~ 4 years without the inlet- α background leaking into a DM signal region.

6. Conclusion

We presented a method that can be used to achieve the background goals in the DEAP-3600 detector with regard to so-called ‘inlet- α s’. The detector inlet is a region of incomplete light collection, and some α -decay events in this region reconstruct in the region of interest for WIMP search. By coating the surface of the inlet with a WLS that has a re-emission time much longer than the LAr singlet state, and then using pulse shape discrimination, we show that it is possible to shift the position in both energy and PSD space where these background events reconstruct, so that they are no longer in the WIMP search window.

The candidate coating for use in this method is composed of 15% pyrene and 85% polystyrene (PPS) by weight, and we describe a procedure for producing a cryogenically stable PPS coating. Characterization results of the photoluminescence response of PPS films were used as input into a toy Monte Carlo simulation and confirm that the photoluminescence quantum yield, emission spectrum, and emission timing are suitable to suppressing inlet- α s.

Future studies will characterize the reflectivity, transparency and refractive index of the film under incident visible light for input in the full-scale GEANT4/ RAT [39, 40] based MC used by DEAP-3600 to determine the inlet- α suppression factor with better precision.

Acknowledgements

We thank the Natural Sciences and Engineering Research Council of Canada, the Canadian Foundation for Innovation (CFI), the Ontario Ministry of Research and Innovation (MRI), Queen’s University, Carleton University, the Canada First Research Excellence Fund, and the Arthur B. McDonald Canadian Astroparticle Research Institute. We acknowledge support from the International Research Agenda Programme AstroCeNT (MAB/2018/7) funded by the Foundation for Polish Science (FNP) from the European Regional Development Fund. AstroCeNT and Technical University of Munich (TUM) cooperation is supported from the EU’s Horizon 2020 research and innovation program under grant agreement No 962480 (DarkWave).

References

- [1] P. A. Amaudruz, M. Baldwin, M. Batygov, et al., Design and construction of the DEAP-3600 dark matter detector, *Astroparticle Physics* 108 (2019) 1–23. doi:10.1016/j.astropartphys.2018.09.006.
URL <https://linkinghub.elsevier.com/retrieve/pii/S0927650518300914>
- [2] P. Agnes, I. F. M. Albuquerque, T. Alexander, et al., DarkSide-50 532-day dark matter search with low-radioactivity argon, *PRD* 98 (2018) 102006. arXiv:1411.4524, doi:10.1103/PhysRevD.98.102006.
URL <https://journals.aps.org/prd/abstract/10.1103/PhysRevD.98.102006>
- [3] A. Hime, The MiniCLEAN Dark Matter Experiment, Proceedings of the DPF Conference (2011). arXiv:1110.1005.
- [4] R. Acciarri, M. Acero, M. Adamowski, et al., Long-Baseline Neutrino Facility (LBNF) and Deep Underground Neutrino Experiment (DUNE) Conceptual Design Report Volume I (2016). arXiv:1601.05471.
- [5] R. Acciarri, C. Adams, R. An, et al., Design and construction of the MicroBooNE detector, *Journal of Instrumentation* 12 (02) (2017) P02017–P02017. doi:10.1088/1748-0221/12/02/p02017.
URL <https://doi.org/10.1088/1748-0221/12/02/p02017>
- [6] I. Nutini, et al., The LArIAT experiment, *Journal of Physics: Conference Series* 888 (2017) 012168. doi:10.1088/1742-6596/888/1/012168.
URL <https://doi.org/10.1088/1742-6596/888/1/012168>
- [7] T. Pollmann, M. Boulay, M. Kuzniak, Scintillation of thin tetraphenyl butadiene films under alpha particle excitation, *NIM A* 635 (1) (2011) 127–130. arXiv:1011.1012, doi:10.1016/j.nima.2011.01.045.
- [8] L. M. Veloce, M. Kuzniak, P. C. F. D. Stefano, et al., Temperature dependence of alpha-induced scintillation in the 1,1,4,4-tetraphenyl-1,3-butadiene wavelength shifter, *JINST* 11 (06) (2016) P06003–P06003. arXiv:1511.08424, doi:10.1088/1748-0221/11/06/P06003.
- [9] C. Stanford, S. Westerdale, J. Xu, F. Calaprice, Surface background suppression in liquid argon dark matter detectors using a newly discovered time component of tetraphenyl-butadiene scintillation, *Physical Review D* 98 (6) (2018) 062002.
- [10] M. G. Boulay, M. Kuzniak, Technique for surface background rejection in liquid argon dark matter detectors using layered wavelength-shifting and scintillating thin films, *Nuclear Instruments and Methods in Physics Research Section A: Accelerators, Spectrometers, Detectors and Associated Equipment* 968 (2020) 163631.
- [11] G. J. Davies, C. H. Lally, W. G. Jones, N. J. T. Smith, UV quantum efficiencies of organic fluors, *NIM B* 117 (1996).
URL http://adsabs.harvard.edu/cgi-bin/nph-data_query?bibcode=1996NIMPB.117..421D&link_type=ABSTRACT

- [12] J. Flournoy, I. Berلمان, B. Rickborn, R. Harrison, Substituted tetraphenylbutadienes as fast scintillator solutes, *Nuclear Instruments and Methods in Physics Research Section A: Accelerators, Spectrometers, Detectors and Associated Equipment* 351 (2) (1994) 349–358. doi: [https://doi.org/10.1016/0168-9002\(94\)91363-3](https://doi.org/10.1016/0168-9002(94)91363-3).
URL <https://www.sciencedirect.com/science/article/pii/0168900294913633>
- [13] B. A. Powell, W. M. Burton, Fluorescence of Tetraphenyl-Butadiene in the Vacuum Ultraviolet, *Applied Optics* 12 (1) (1973) 87–89. doi: [10.1364/AO.12.000087](https://doi.org/10.1364/AO.12.000087).
- [14] V. Boccone, P. K. Lightfoot, K. Mavrokoridis, et al., Development of wavelength shifter coated reflectors for the ArDM argon dark matter detector, *Journal of Instrumentation* 4 (06) (2009) P06001–P06001. arXiv:0904.0246, doi: [10.1088/1748-0221/4/06/p06001](https://doi.org/10.1088/1748-0221/4/06/p06001).
- [15] M. Clark, M. Kuźniak, M. Zheng, P. Di Stefano, Spectroscopic and time-resolved measurements of the fluorescence of pyrene at low temperatures for noble liquid particle detectors, presented at CAP 2016, <https://indico.cern.ch/event/472838/contributions/1150228> (2016).
- [16] D. McKinsey, C. Brome, J. Butterworth, et al., Fluorescence efficiencies of thin scintillating films in the extreme ultraviolet spectral region, *Nucl. Instrum. Methods Phys. Res. B* 132 (3) (1997) 351 – 358. doi: [10.1016/S0168-583X\(97\)00409-6](https://doi.org/10.1016/S0168-583X(97)00409-6).
URL <http://www.sciencedirect.com/science/article/pii/S0168583X97004096>
- [17] M. Kuzniak, B. Broerman, T. Pollmann, G. R. Araujo, Polyethylene naphthalate film as a wavelength shifter in liquid argon detectors, *The European Physical Journal C* 79 (2019) 291. doi: [10.1140/epjc/s10052-019-6810-8](https://doi.org/10.1140/epjc/s10052-019-6810-8).
URL <http://link.springer.com/10.1140/epjc/s10052-019-6810-8>
- [18] M. Kuźniak, A. M. Szelc, Wavelength shifters for applications in liquid argon detectors, *Instruments* 5 (1) (2021) 4.
- [19] J. B. Birks, A. A. Kazzaz, T. A. King, B. H. Flowers, 'excimer' fluorescence - ix. lifetime studies of pyrene crystals, *Proc. R. Soc. Lond. A* 291 (1427) (1966) 556–569. doi: [10.1098/rspa.1966.0114](https://doi.org/10.1098/rspa.1966.0114).
URL <https://royalsocietypublishing.org/doi/abs/10.1098/rspa.1966.0114>
- [20] B. Broerman, M. G. Boulay, B. Cai, et al., Application of the TPB Wavelength Shifter to the DEAP-3600 Spherical Acrylic Vessel Inner Surface, *Journal of Instrumentation* 12 (2017) 04017. arXiv:1704.01882, doi: [10.1088/1748-0221/12/04/p04017](https://doi.org/10.1088/1748-0221/12/04/p04017).
- [21] W. Sonnefeld, W. Zoller, W. May, Dynamic coupled-column liquid-chromatographic determination of ambient-temperature vapor pressures of polynuclear aromatic hydrocarbons, *Analytical Chemistry* 55 (2) (1983) 275–280.
- [22] G. E. Johnson, Effect of Concentration on the Fluorescence Spectra and Lifetimes of Pyrene in Polystyrene Films, *Macromolecules* 13 (1980) 839.
- [23] A. Itaya, T. Yamada, K. Tokuda, H. Masuhara, Interfacial characteristics of poly (methyl methacrylate) film: aggregation of pyrene and micropolarity revealed by time-resolved total internal reflection fluorescence spectroscopy, *Polymer journal* 22 (8) (1990) 697–704.
- [24] K. Procházka, Historical perspective of advances in fluorescence research on polymer systems, in: K. Procházka (Ed.), *Fluorescence Studies of Polymer Containing Systems*, 1st Edition, Springer, Switzerland, 2016, p. 180.
- [25] R. Ajaj, P. A. Amaudruz, G. R. Araujo, et al., Search for dark matter with a 231-day exposure of liquid argon using DEAP-3600 at SNOLAB, *PRD* 100 (2019) 022004. arXiv:1902.04048, doi: [10.1103/PhysRevD.100.022004](https://doi.org/10.1103/PhysRevD.100.022004).
- [26] D. Gallacher, M. Boulay, Surface background rejection technique for liquid argon dark matter detectors using a thin scintillating layer, *Journal of Instrumentation* 15 (03) (2020) C03016–C03016.
- [27] M. Clark, P. Nadeau, S. Hills, et al., Particle detection at cryogenic temperatures with undoped csi, *Nuclear Instruments and Methods in Physics Research Section A: Accelerators, Spectrometers, Detectors and Associated Equipment* 901 (2018) 6–13. doi: <https://doi.org/10.1016/j.nima.2018.05.066>.
URL <https://www.sciencedirect.com/science/article/pii/S0168900218306855>
- [28] H. Benmansour, Characterization of pyrene films for background rejection in liquid argon dark matter experiments, Master's thesis (2021).
URL <http://hdl.handle.net/1974/28962>
- [29] G. R. Araujo, T. Pollmann, A. Ulrich, Photoluminescence response of acrylic (PMMA) and polytetrafluoroethylene (PTFE) to ultraviolet light, *The European Physical Journal C* 79 (2019) 635. doi: [10.1140/epjc/s10052-019-7152-2](https://doi.org/10.1140/epjc/s10052-019-7152-2).
URL <http://link.springer.com/10.1140/epjc/s10052-019-7152-2>
- [30] A. Leonhardt, Characterization of wavelength shifters for rare-event search experiments with a vuv spectrofluorometer, Master's thesis, Technical University of Munich (TUM) (07 2021). doi: [10.13140/RG.2.2.25067.87849](https://doi.org/10.13140/RG.2.2.25067.87849).
- [31] R. Francini, et al., Tetraphenyl-butadiene films: VUV-Vis optical characterization from room to liquid argon temperature, *JINST* 8 (2013) C09010. doi: [10.1088/1748-0221/8/09/C09010](https://doi.org/10.1088/1748-0221/8/09/C09010).
- [32] M. G. Boulay, V. Camillo, N. Canci, et al., Direct comparison of PEN and TPB wavelength shifters in a liquid argon detector (2021). arXiv:2106.15506.
- [33] P. Adhikari, R. Ajaj, G. R. Araujo, et al., The liquid-argon scintillation pulse shape in DEAP-3600, *EPJ C* 80 (4) (2020) 506. arXiv:2001.09855v2, doi: [10.1140/epjc/s10052-020-7789-x](https://doi.org/10.1140/epjc/s10052-020-7789-x).
- [34] D. Brown, M. Chadwick, R. Capote, et al., Endf/b-viii.0: The 8th major release of the nuclear reaction data library with cielo-project cross sections, new standards and thermal scattering data, *Nuclear Data Sheets* 148 (2018) 1–142, special Issue on Nuclear Reaction Data. doi: <https://doi.org/10.1016/j.nds.2018.02.001>.
URL <https://www.sciencedirect.com/science/article/pii/S0090375218300206>
- [35] P. A. Amaudruz, M. Batygov, B. Beltran, et al., In-situ characterization of the Hamamatsu R5912-HQE photomultiplier tubes used in the DEAP-3600 experiment, *NIM A* 922 (2019) 373–384. arXiv:1705.10183, doi: [10.1016/j.nima.2018.12.058](https://doi.org/10.1016/j.nima.2018.12.058).
- [36] J. F. Ziegler, M. D. Ziegler, J. P. Biersack, SRIM - The stopping and range of ions in matter (2010), *Nuclear Instruments and Methods in Physics Research B* 268 (11-12) (2010) 1818–1823. doi: [10.1016/j.nimb.2010.02.091](https://doi.org/10.1016/j.nimb.2010.02.091).
- [37] A. Hitachi, A. Mozumder, Properties for liquid argon scintillation for dark matter searches (2019). arXiv:1903.05815.
- [38] P. Adhikari, R. Ajaj, M. Alpizar-Venegas, et al., Pulse shape discrimination against low-energy ar-39 beta decays in liquid argon with 4.5 tonne-years of deap-3600 data (2021). arXiv:2103.12202.

- [39] S. Agostinelli, J. Allison, K. Amako, et al., Geant4—a simulation toolkit, *Nuclear Instruments and Methods in Physics Research Section A: Accelerators, Spectrometers, Detectors and Associated Equipment* 506 (3) (2003) 250–303. doi:[https://doi.org/10.1016/S0168-9002\(03\)01368-8](https://doi.org/10.1016/S0168-9002(03)01368-8).
URL <https://www.sciencedirect.com/science/article/pii/S0168900203013688>
- [40] T. Bolton, et al., *RAT (is an Analysis Tool) User's Guide*, *RAT (is an Analysis Tool) User's Guide* (2018).
URL <https://rat.readthedocs.io/>